Nature of the Interfaces Between Stoichiometric and Under-Stoichiometric MoO_3 and 4,4′-*N*,*N*′-dicarbazole-biphenyl: A Combined Theoretical and Experimental Study

*Theodoros A. Papadopoulos, Jens Meyer, Hong Li, Zelei Guan, Antoine Kahn, and Jean-Luc Brédas**

A combination of density functional theory and experimental measurements via ultraviolet and X-ray photoelectron spectroscopies is used to explore the nature of the interface between the stoichiometric molybdenum trioxide (MoO_3) or its under-stoichiometric counterpart with oxygen vacancies, and an organic hole-transport layer represented by 4,4′-*N*,*N*′-dicarbazole-biphenyl (CBP). Upon adsorption of CBP, special attention is paid to i) the appearance of gap states and the reduction of the molybdenum oxide surface, and ii) the evolution of the work function. Very good agreement is found between theory and experiment. The near alignment of the CBP highest occupied molecular orbital with the Fermi level and the conduction band edge of molybdenum oxide points to facile hole collection or injection.

1. Introduction

Over the past two decades, transition metal oxides (TMO) such as molybdenum or tungsten tri-oxide (MoO_3, WO_3) have been extensively studied because of their broad range of applications as hole-injection or hole-extraction layer in organic light-emitting diodes (OLED) and organic photovoltaic (OPV) cells, respectively.[1] Recently, the electronic structure of these two TMOs has been investigated by ultra-violet photoelectron spectroscopy (UPS) and inverse photoemission spectroscopy (IPES), which led to three remarkable observations:[2] first, their electronic structures are nearly identical; second, they exhibit exceptionally large work functions of >6.5 eV; and third, they show an n-type behavior, placing the Fermi level just a few hundred meV below the conduction band minimum (CBM).

Most reports on TMOs focus on a macroscopic perspective and describe device characteristics in due consideration of the energetics. For example, Subbiah et al.[3] attributed the reduced series resistance of an OPV cell with an MoO_3 interlayer to band bending at the TMO-aluminum phthalocyanine chloride (AlPcCl) interface as measured via UPS. More recently, a model for charge injection via MoO_3 was proposed by Kröger et al.[4] based on the observation of the very large oxide work-function and interface dipole at the *N*,*N*′-di[(1-naphthyl)-*N*,*N*′-diphenyl]-1,1′-biphenyl-4,4′-diamine (α-NPD)/MoO_3 interface. The high work function of the oxide results in a charge transfer from the organic semiconductor to the oxide and a small energy barrier between the oxide conduction band minimum and the highest occupied molecular orbital (HOMO) of the organics. Even though these studies have led to a much better understanding of the role of TMOs in organic electronic devices, a detailed microscopic description of the TMO/organic interface remains to be reached.

Here, we seek to provide such a molecular understanding by examining the adsorption on a molybdenum oxide surface of π-conjugated organic molecules representing an organic hole-transport layer. We discuss the effect of both stoichiometric and under-stoichiometric metal oxide surfaces on the energy level alignment with the hole-transport layer. The enhancement of the experimentally observed gap-state density[5,6] after adsorption of the organic films on the metal oxides is also evaluated. These questions are of particular importance for a thorough understanding of the effectiveness of TMOs to further improve the performance of organic electronic devices.

In the present work, we investigate a representative interfacial system MoO_3/4,4′-*N*,*N*′-dicarbazole-biphenyl (CBP) (**Figure 1**) via a joint experimental and theoretical analysis. We consider both stoichiometric and under-stoichiometric MoO_3 surfaces and their interfaces with CBP. We observe that oxygen

Dr. T. A. Papadopoulos,[+] Dr. H. Li, Prof. J.-L. Brédas
School of Chemistry and Biochemistry and Center for Organic Photonics and Electronics
Georgia Institute of Technology
Atlanta, GA 30332-0400, USA
E-mail: jean-luc.bredas@chemistry.gatech.edu
Dr. J. Meyer,[++] Dr. Z. Guan, Prof. A. Kahn
Department of Electrical Engineering
Princeton University
Princeton, NJ 08544, USA
[+]Present address: Institut de Physique, Université de Liège, B-4000, Liège, Belgium
[++]Present address: Philips Research, Weisshausstrasse 2, D-52066 Aachen, Germany

DOI: 10.1002/adfm.201301466

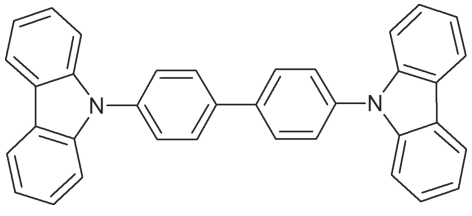

Figure 1. The chemical structure of 4,4′-*N*,*N*′-dicarbazole-biphenyl (CBP).

vacancies shift the Fermi level (E_F) upwards in energy very close to the CB edge in the under-stoichiometric case, while in the stoichiometric case, a shift of the Fermi energy is observed upon adsorption of CBP. As a result, the deep-lying CB makes both the stoichiometric and under-stoichiometric MoO_3 surfaces a suitable interlayer to collect electrons from the CBP HOMO. Regardless of the appearance of gap states, the HOMO and HOMO-1 of the adsorbate are found to be located right below the CB edge, which is consistent with the UPS measurements, about 0.2 eV below the CB edge. Thus, gap states due to different types of oxygen vacancies are not essential to realize efficient hole-injection and hole-collection at such inorganic/organic interfaces.

2. Methodology

2.1. Experimental

MoO_3 and CBP films were thermally evaporated in an ultra-high vacuum (UHV) growth chamber (10^{-9} Torr) and transferred to an analysis chamber (<10^{-10} Torr) without breaking vacuum. MoO_3 was evaporated from a temperature-controlled Knudsen cell at around 420 °C, while CBP was sublimated from a simple quartz crucible. Deposition rates and total thicknesses were monitored via a quartz microbalance. UPS was carried out with both He I (21.22 eV) and He II (40.8 eV) radiation lines from a discharge lamp to study the electronic structure of MoO_3 and the energy level alignment with CBP, with an experimental resolution of 0.15 eV. X-ray photoelectron spectroscopy (XPS) was conducted to analyze the core levels of MoO_3, for composition and chemical analysis, using the Al Kα (1486.6 eV) photon line with a spectral resolution of 0.8 eV.[7]

2.2. Theoretical

The slab approach was used for all systems. Calculations on both the stoichiometric MoO_3(010) and n-type under-stoichiometric MoO_x(010) (x = 2.94) slabs with and without adsorption of CBP were carried out at the density functional theory (DFT) level with plane-wave basis sets using the Vienna Ab Initio Simulation Package (VASP).[8] Periodic boundary conditions were implemented giving rise to an infinite interface on the x–z plane; a vacuum space of ≈45 Å was enforced between each repeated slab along the y-axis. The Perdew-Burke-Ernzerhof (PBE) gradient-corrected exchange-correlation functional was used;[9] all calculations were performed using the projector augmented wave (PAW) method[10] with a plane-wave cut-off energy of 400 eV and a Γ-centered k-point grid of 2 × 1 × 4 for the CBP-covered MoO_3 and MoO_x surfaces and 6 × 2 × 6 for the bare surfaces. A Gaussian smearing with a width of 0.05 eV was used to determine how partial occupancies are set for each wavefunction.

The bulk crystal MoO_3 presents an orthorhombic layer structure (a = 3.963 Å, b = 13.855 Å, and c = 3.696 Å) with each unit cell containing two Mo–O bilayers[11] parallel to the (010) crystal face, which is the most exposed and thermodynamically

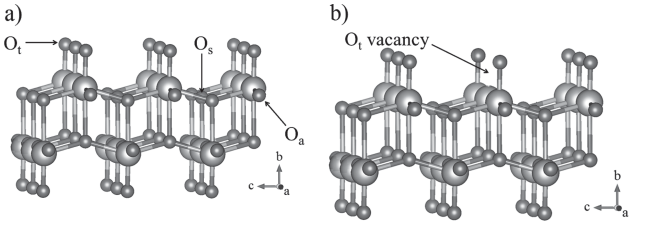

Figure 2. a) Bilayer surface structure of MoO_3(010); the different types of oxygen atoms are indicated. b) MoO_x(010) with a terminal O_t vacancy site. Mo atoms are presented in light gray and O atoms in dark gray.

stable surface[12] (see Figure S1 in the Supporting Information). Since each bilayer interacts with the neighboring bilayers through noncovalent van der Waals forces, even a small overestimation or underestimation of the van der Waals contribution could cause a large error in the equilibrium geometry;[13] hence, we chose to model the MoO_3(010) and MoO_x(010) substrates by a slab containing a single Mo–O bilayer based on the crystal structure defined in another study;[11] we have used this crystal structure as the initial coordinates for the optimization of the MoO_3 bilayer slab. All Mo and O atoms were allowed to relax apart from the lowest terminal oxygen atoms that were kept fixed at their crystallographic coordinates representing "bulk" MoO_3. In addition, atom coordinates along the b direction were kept fixed at their experimental values, as done elsewhere.[14]

As mentioned in other relevant work,[14–16] there are three types of crystallographically distinct O atoms in the vicinity of a Mo atom. These are referred to as terminal (O_t), asymmetric (O_a), and symmetric (O_s) oxygen atoms (**Figure 2**a), with their distance to the Mo atom optimized to be 1.67 Å for O_t, 1.76 Å and 2.22 Å for O_a, and 1.95 Å (two equivalent bonds) and 2.34 Å for O_s.

The unit cell of the slab for the MoO_3/CBP system is constructed with double the size of the bare MoO_3 slab to accommodate the organic adsorbate; the same holds for the MoO_x/CBP slab. The DFT-optimized structure of the CBP monolayer adsorbed on the MoO_3 surface is shown in **Figure 3**. The CBP molecules were added on the metal-oxide surface with an average lateral distance of about 5 Å between the nearest-neighboring molecules after relaxation, equivalent to a surface density of 3.79 × 10^{13} molecules per cm^2; steric effects

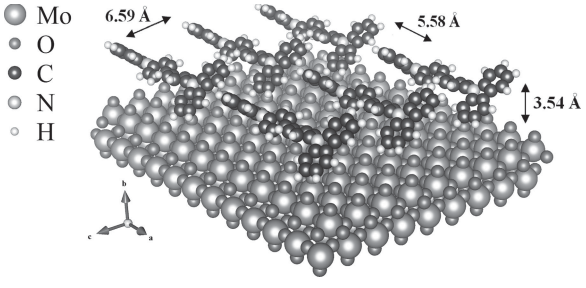

Figure 3. CBP physisorbed on the MoO_3(010) surface with coverage density ρ = 3.79 × 10^{13} cm^{-2}. The distances of 5.58 Å and 6.59 Å are between the closest H atoms of two adjacent CBP molecules along the x and z axes, respectively; the distance of 3.54 Å is between the closest H of CBP to the O atom of the MoO_3 slab.

are hence avoided between neighboring molecules. The distance between MoO_3 and the CBP backbone was optimized and found to be ≈6.01 Å. When this distance is defined as the average distance of the two N atoms of CBP with the plane corresponding to the uppermost terminal oxygen atoms, the distance of each N atom with its closest Mo atom was found, after optimization, to be 7.79 Å and 7.62 Å (the closest distance between a hydrogen atom of CBP and an oxygen atom of the slab is 3.54 Å).

Oxygen vacancies were introduced after the optimizations of the stoichiometric MoO_3 and MoO_3/CBP slabs were finalized. The oxygen vacancy sites were created by removing one O atom per unit cell from the bare MoO_3 slab (see Figure 2b for illustration of a terminal O vacancy), which is equivalent to removing two O atoms from the MoO_3/CBP interface slab unit cell (the $x = 2.94$ stoichiometry for the MoO_x/CBP slab thus corresponds to a unit cell with 36 Mo and 106 O atoms). The oxygen vacancies for the latter case are initially located right below the two N atoms of CBP, and the coordinates of the new bare MoO_x and MoO_x/CBP slabs were re-optimized. After the new optimization was completed, the distance between MoO_x and the CBP backbone, as defined above, was found to be ≈5.95 Å. The distance between the first and second N atom of CBP and their closest Mo atom was found to be 7.68 Å and 7.60 Å respectively. Illustrations of the structures and charge densities in this work are based on the visualization tool VESTA.[17]

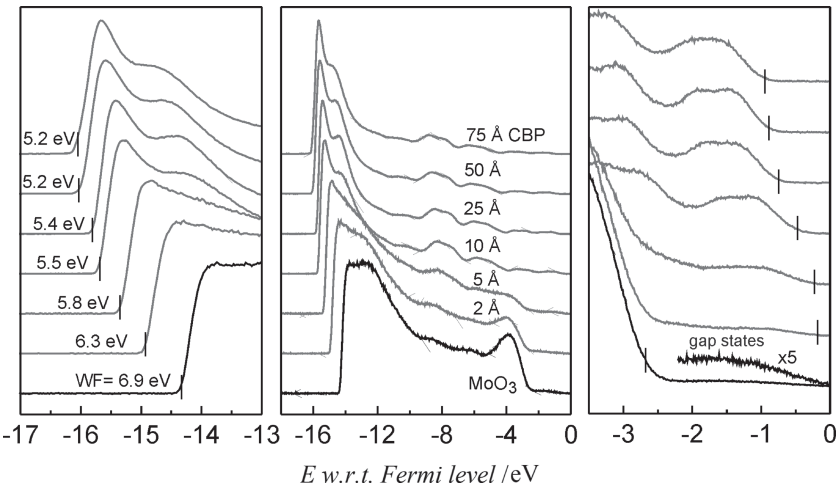

Figure 4. UPS spectra of MoO_3 and of CBP films on MoO_3 plotted with respect to Fermi level. Left panel: magnified view of the photoemission cut-off. Central panel: full UPS spectra. Right panel: magnified view of the valence band states near the Fermi level.

3. Results and Discussion

3.1. Experimental Measurements

MoO_3 films evaporated in vacuum were deposited on ITO followed by the CBP deposition. The smallest nominal CBP thickness observed via UPS measurements is 2 Å, corresponding to a fraction of a monolayer. We note that the calculations indicate that the orientation of the CBP long axis is parallel with respect to the MoO_3(010) surface; the backbone length of the optimized geometry of CBP was found to be equal to 9.96 Å (N to N distance).

Figure 4 displays the UPS spectra of CBP films on MoO_3(010) with increasing thickness from 2 to 75 Å. The photoemission cut-off (left panel) of MoO_3 is found at 14.3 eV, which corresponds to a work function of 6.9 eV. The valence band maximum (VBM) is located at 2.8 eV below the Fermi level (right panel) resulting in an ionization energy (IE) of 9.7 eV. We observe that a few Å of CBP deposited on MoO_3 cause a rapid decrease of the work function, as seen from the shift of the photoemission cut-off towards higher binding energies. The work-function reduction is ≈0.63 eV for a 2 Å sub-monolayer of CBP, and reaches 1.7 eV for a thickness of about 50 Å. A closer look at the energy region near the Fermi level (Figure 4, right panel) shows a broad set of gap states in the MoO_3 spectra (highlighted through five-fold magnification), which is centered near –1.4 eV and extends up to the Fermi level. Upon CBP deposition, the onset of the molecular HOMO starts very close to E_F and progressively moves away with increasing layer thickness.

The significant decrease of the MoO_3 work function with increasing CBP layer thickness represents a downward shift of the vacuum level. The initial decrease corresponds to a large interface dipole, as will be theoretically quantified below. The progressive shift of the valence and HOMO levels away from E_F can be seen as band bending, which is related to a p-doping effect of CBP at the very interface between MoO_3 and the CBP molecules. Because of the large initial work-function of MoO_3, electron transfer takes place at the interface from the organic molecules to the oxide (see below), as has been proposed by Kröger et al.[4] Band bending occurs as a result of a strongly p-doped organic interface and of the HOMO level moving away from E_F due to the absence of charge transfer from the bulk of the molecular film. At the interface, as the HOMO level of CBP is nearly pinned at E_F and MoO_3 is an n-type material, Kröger et al. proposed that charge transfer occurs via electron extraction from the HOMO of CBP to the conduction band minimum of MoO_3. Further details can be found in the recent review by Meyer et al.[5]

We now turn to a discussion of the gap state formation in the oxide via an XPS analysis. **Figure 5**a shows the evolution of the Mo 3d core level peak upon CBP adsorption. The MoO_3 film features two peaks at 232.7 eV and 235.8 eV, related to the 3d 3/2 and 5/2 components of the core level, with a ≈3.1 eV spin-orbit splitting and corresponding to a nearly stoichiometric (Mo^{6+}) oxide composition. With a few adsorbed CBP molecules, two additional peaks arise at 234.4 eV and 231.6 eV and increase in intensity with increasing layer thickness. The positions of the additional two peaks are consistent with the Mo^{5+} oxidation state. Thus, the deposition of CBP appears to induce a reduction process of MoO_3 at the very interface. These reduced MoO_x species are at the origin of the increased gap state density shown in the UPS spectra. It is worth mentioning that Kanai

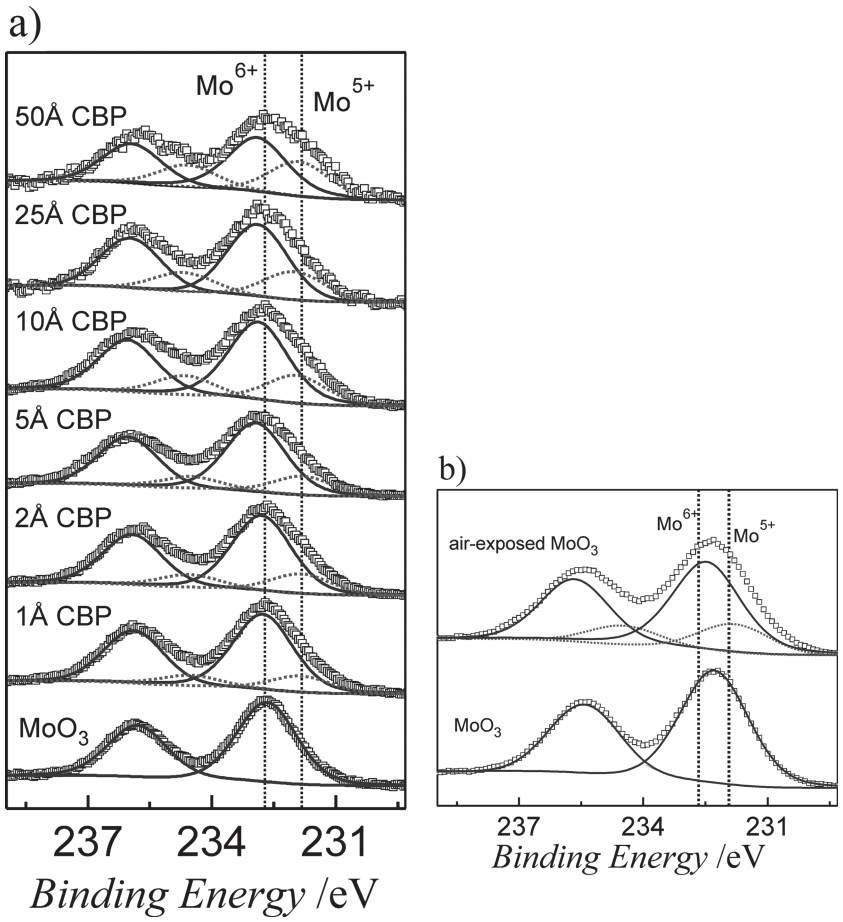

Figure 5. a) XPS spectra of the Mo 3d core level upon CBP adsorption. b) XPS spectra of the Mo 3d core level before and after a 15 min air exposure. The dotted and solid lines correspond to the Mo^{5+} and Mo^{6+} peak fitting curves, respectively.

et al.[18] identified an increasing gap state density when an α-NPD film is adsorbed on a MoO_3 surface. Furthermore, Greiner et al.[19] demonstrated that gap state formation increases in thin film MoO_3 with increasing oxygen vacancy concentration. Also, as shown in the literature,[20] O_2-plasma treatment reduces the amount of gap states as well as Mo^{5+} states, which confirms that indeed reduced MoO_x species are related to gap state formation.

Other observations also pertain to the TMO work function and stoichiometry. It has been observed that the high TMO work function is highly sensitive to, and decreases rapidly with, ambient exposure.[21,22] However, short exposure times, as well as full solution-processing, still lead to TMO films with remarkable hole-injection and hole-extraction properties.[21,23] Vacuum annealing of exposed TMO films also results in a nearly full recovery of the energetics of freshly evaporated thin films.[24] The increased gap state density, which is caused by a partial reduction process from Mo^{6+} to Mo^{5+} at the metal oxide surface, is most likely induced by adsorbed hydrocarbon species when samples are air-exposed, leading to a similar charge transfer as discussed above. In Figure 5b, we show that air exposure of freshly evaporated MoO_3 changes drastically the surface stoichiometry, as seen in the rise of a significant amount of Mo^{5+} states. By comparing these results with those of Figure 5a, it appears that the chemical composition of MoO_3 briefly exposed to air (15 min) shows strong similarity with that induced by the deposition of a fraction of a monolayer of CBP.

3.2. DFT Calculations

To explore the origin of the gap states observed in both UPS and XPS measurements and the change in surface electronic structure and work-function upon adsorption of the CBP molecules, we carried out DFT calculations using the theoretical procedure described in the methodology section.

3.2.1. MoO_3 and MoO_x Bare Surfaces

The crystal bilayer structure of the stoichiometric MoO_3 bare surface is included in Figure 2a. The calculated DOS shows a band gap of 2.13 eV (see **Figure 6**a); this value is some 0.9 eV smaller than the experimental value of ≈3.0 eV,[21] which is related to the well-known limitation of conventional DFT that tends to underestimate the band gap for semiconductors and insulators. We observe that the top valence bands mainly consist of O 2p levels with nearly no contribution from Mo 4d levels. This is confirmed by the illustration of the partial charge density corresponding to states 0.15 eV below E_F (Figure 6b), which clearly shows that the charge density there is distributed around O atoms. On the other hand, the bottom of the conduction band consists of a major contribution from Mo 4d states

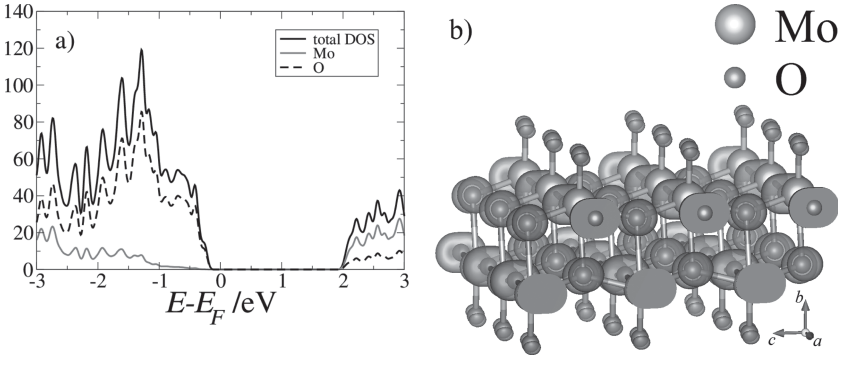

Figure 6. a) Total density of states (solid black line), as well as individual contributions from Mo (solid gray line) and O atoms (dashed line) for the bare MoO_3 surface. b) Charge density corresponding to states 0.15 eV below the E_F; the cross-sections formed (ovals) when the charge density isosurface is cut by a unit cell edge are also visible.

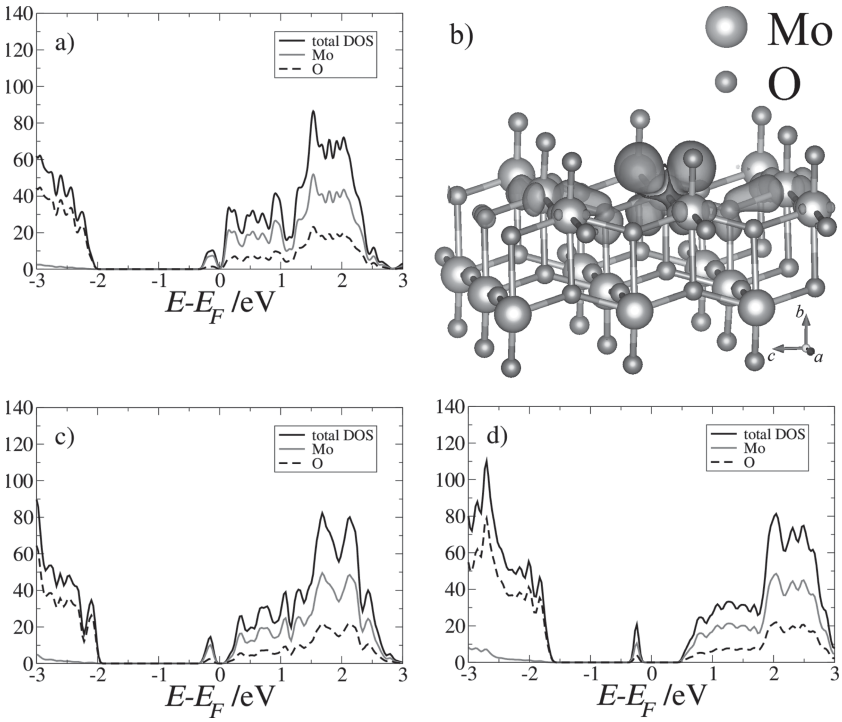

Figure 7. a) Total density of states (solid black line) as well as individual contributions from Mo (solid gray line) and O (dashed line) atoms of the bare surface of MoO_x showing an n-type semiconductor behavior for a terminal O vacancy and b) its DOS projected partial charge on the oxygen vacancy states. c) DOS and PDOS for an asymmetric O vacancy and d) for a symmetric O vacancy.

and a smaller contribution of O 2p states. The calculated band gap is consistent with earlier DFT calculations at the PBE level of theory for bulk MoO_3, which presented an indirect band gap of 1.95 eV.[16]

Figure 2b illustrates the bilayer structure of the under-stoichiometric MoO_x (010) surface, that is, with one oxygen vacancy per slab leading to $x = 2.94$; such low oxygen vacancy concentrations have also been observed by Cho et al.[25] via soft X-ray spectroscopy. While we have considered asymmetric and symmetric oxygen vacancies as well, here, we have chosen to focus on the terminal oxygen vacancies when considering the MoO_x/CBP interface systems, since they reflect the strongest interactions with the adsorbed CBP layer due to closer proximity.

The total DOS, as well as the projected density of states (PDOS) from individual contributions of Mo and O atoms of the bare MoO_x surface with a terminal O vacancy, are shown in **Figure 7**a. Distinct from the case of the MoO_3 surface, the DOS for the bare MoO_x surface with a terminal vacancy shows a shallow electron-donor state at ≈0.1 eV below the CB edge, which displays a major contribution from Mo 4d states and a small hybridization with O 2p states. To further investigate the origin of this state, we plot in Figure 7b its corresponding partial charge density. It is found to be strongly localized on the Mo atom right below the oxygen vacancy, since the removal of an oxygen atom leaves the neighboring Mo atoms with "dangling bonds".

We note that the DOS of the bare MoO_x surface with an asymmetric oxygen vacancy (Figure 7c) shows similar features with the DOS of a terminal vacancy; the main difference is that the electron-donor states due to the asymmetric vacancy are about 0.3 eV below the CB edge. Thus, it appears that O_t and O_a vacancies are contributing to the experimentally observed gap states near the Fermi energy. When considering the symmetric oxygen vacancy (Figure 7d), we observe a distinct peak, located almost at mid-gap, ≈0.75 eV below the CB edge, with contributions from Mo 4d and O 2p levels similar to those for the O_t and O_a vacancies. We thus obtain both shallow and deep donor states on the bare MoO_x surfaces, with the former related to O_t and O_a vacancies and the latter to O_s vacancies. As such, we can infer that in practice a combination of different types of vacancies could induce a complex geometry and hence complex energetics especially if vacancies are created in more "bulk-like" locations, that is, in deeper layers within the MoO_x film. This situation would be consistent with the broad range of gap states observed experimentally via UPS, centered at ≈1.4 eV below E_F but extending up to E_F (Figure 4).

The electron affinity (EA), ionization energy (IE), and work function for the bare MoO_3(010) and MoO_x(010) surfaces with an O_t vacancy are given in **Table 1**. Since the bare MoO_3 surface model is an intrinsic semiconductor, there are no available experimental data to compare with; we therefore only present its EA and IE values here and compare them with the experimentally measured values of the n-type MoO_x. The EA and IE values for both intrinsic and n-type surface models are, as expected, smaller than the experimental values, a feature again related to the fact that conventional DFT tends to underestimate the band gap. The calculated work function for the n-type MoO_x surface with an O_t vacancy is 6.2 eV, which is 0.7 eV lower than the experimental value. A similar trend was observed in our earlier modeling of the indium tin oxide (ITO) surface, where the calculated work-function is more than 1 eV lower than the experimental value.[26] However, since we are mainly interested in the change in work-function caused by the molecular deposition, the difference in the absolute value does not affect the conclusions drawn from the theoretical modeling; this point was demonstrated in our

Table 1. Comparison of the electron affinities (EA) and ionization energies (IE) of the MoO_3(010) and MoO_x(010) bare surfaces between our theoretical results and the experimental values published elsewhere.[2] The MoO_x(010) bare surface slab contains a single O_t vacancy per unit cell.

	MoO_3		MoO_x		
	EA [eV]	IE [eV]	EA [eV]	IE [eV]	E_F [eV]
Theory	6.3	8.6	6.0	8.2	6.2
Experiment[2]	–	–	6.7	9.7	6.9

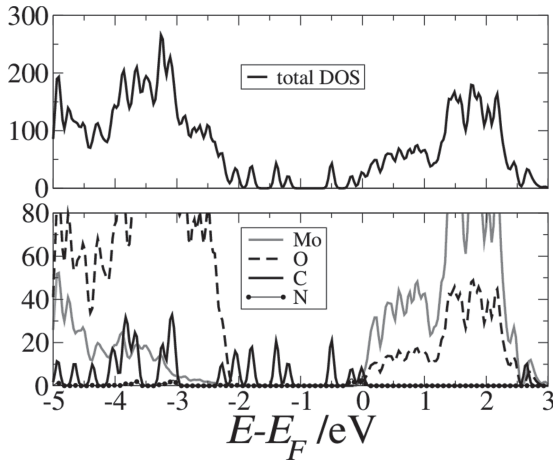

Figure 8. Total density of states (upper panel) as well as individual contributions from Mo, O, C, and N atoms of the MoO_3/CBP interface (lower panel).

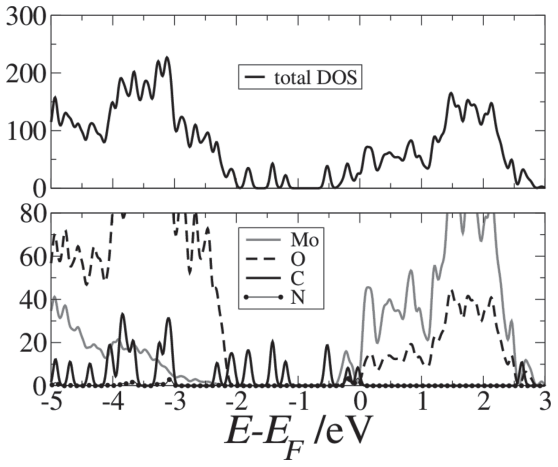

Figure 9. Total density of states (upper panel) as well as individual contributions from Mo, O, C, and N atoms of the MoO_x(010)/CBP interface (lower panel).

earlier work on surface modification of ITO by a series of phosphonic acid molecules.[27]

3.2.2. Energy-Level Alignment at MoO_3/CBP and MoO_x/CBP Interfaces

In comparison to the DOS for the bare MoO_3 surface (Figure 6a), the projected density of states for the combined MoO_3/CBP system (**Figure 8**) presents similar Mo 4d and O 2p contributions as well as distinct peaks originating in the CBP molecules. The CBM and VBM of the MoO_3 slab are located at the E_F (0.0 eV) and –2.1 eV, respectively, corresponding to a band gap of ≈2.1 eV for the MoO_3 surface slab. The frontier molecular orbitals associated with the CBP molecules are distributed within the band gap of MoO_3, with the HOMO aligned with the CBM of MoO_3 at the E_F for the MoO_3/CBP interface, with the nearly degenerate HOMO-1 located ≈0.16 eV below the HOMO. This is consistent with the UPS measurements, showing the HOMO of CBP very close to the CBM. The molecular characters of both HOMO and HOMO-1 are confirmed by comparing them with the HOMO and HOMO-1 levels of the isolated CBP. Their energy difference is also close to the HOMO and HOMO-1 energy difference of the isolated CBP, calculated to be 0.14 eV.

As mentioned above, we have primarily considered an O_t vacancy to the MoO_x/CBP interface as it is located within the uppermost O layer and, hence, the oxygen vacancy is expected to strongly interact with the adsorbate due to close proximity. The DOS of the MoO_x/CBP (x = 2.94) interface (**Figure 9**) appears very similar to that of the MoO_3/CBP interface (Figure 8), except for the levels right below the E_F level. The PDOS (lower panel of Figure 9) shows that these are highly mixed levels associated with contributions of both the molybdenum atoms from the MoO_x slab and the carbon and nitrogen atoms belonging to the CBP molecules. The charge distribution corresponding to these levels is shown in **Figure 10**, with the level aligned with E_F corresponding to the CBP HOMO (Figure 10a), and the state right below the HOMO representing

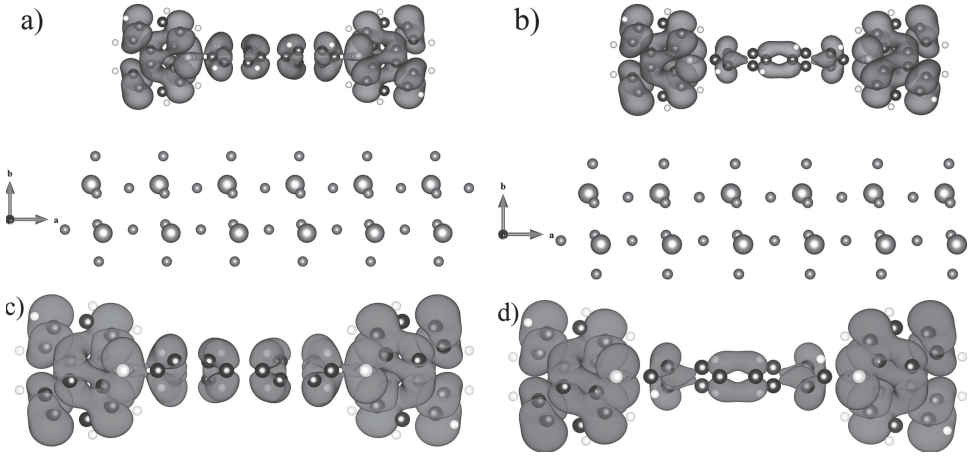

Figure 10. Electron charge densities corresponding to a) the HOMO and b) HOMO-1 levels of the CBP molecule in the MoO_x/CBP system, and c) the HOMO and d) HOMO-1 of an isolated CBP monolayer.

a mixed level consisting of the CBP HOMO-1 and Mo 4d orbitals associated with the O_t oxygen vacancies (Figure 10b). The C-based levels in the gap are related to lower occupied molecular orbitals (Figures 8,9), which partly correspond to the gap levels observed experimentally after adsorption (Figure 4). It is not only the O vacancies that push the Fermi level close to the CB edge (Figure 7) but also the adsorbate itself (Figure 8) as observed experimentally in earlier works.[19,21] We hence infer that both the oxygen vacancies and the organic adsorbate contribute to the formation of gap states at MoO_3 surfaces upon CBP deposition. According to our model, charge transfer takes place via the CB of MoO_x (see the next section). It thus seems that the existence of gap states is not essential to realize an efficient hole-injection or hole-collection process; they are important, nevertheless, since they are related to the n-doping of the MoO_x surface to make it conductive. Since MoO_x interfacial layers are in general very thin (1–5 nm) when used in organic device applications, an n-doped surface might also contribute to increase the bulk conductivity.

3.2.3. Work-Function Change at MoO_3 and MoO_x Surfaces due to CBP Adsorption

As shown in Figure 4 via the UPS measurements, the work-function change of the MoO_3 surface induced by a thin CBP layer of ≈2 to 5 Å is –0.95 eV. Our calculated work-function change with respect to the MoO_3 surface (using the DFT-calculated EA for MoO_3 as a reference here) is found to be –1.22 eV, in line with the UPS measurements. Interestingly, the work-function change calculated for the under-stoichiometric MoO_x surface modified by the CBP monolayer is –1.11 eV, very close to the value obtained for the stoichiometric MoO_3 surface. This is consistent with the trend observed in the DOS calculations for both MoO_3/CBP and MoO_x/CBP interfaces, suggesting that the CBP monolayer has the same effect on both stoichiometric and under-stoichiometric MoO_3 surfaces. From this result, we can conclude that Fermi level pinning and n-doping of molybdenum trioxide is not only related to the stoichiometry of MoO_x, which is suggested in several reports,[18,28] but also to the adsorption of an organic monolayer on the TMO surface.

As extensively discussed in our earlier work on the modification of metal or metal-oxide surfaces by organic molecular layers,[29] the total work-function change $\Delta\Phi$ of a metal or metal-oxide surface can be generally decomposed into three independent components, coming from i) the electrostatic potential energy step ($\Delta V_{mol.}$) across the molecular layer, ii) the potential energy change at the very interface between the molecular layer and the surface ($\Delta V_{int.dip.}$) related to the interface dipole, and iii) the work-function change of the bare surface caused by surface geometry relaxation upon deposition of the molecular layer($\Delta V_{geo.rel.}$).

In the two interface systems discussed here, the contribution of $\Delta V_{mol.}$ to the total work-function change, which is related to the potential energy step across an isolated CBP monolayer at the same geometry as the one optimized for the combined system, is approaching zero (0.01 and 0.0 eV for the MoO_3/CBP and MoO_x/CBP, respectively). This is due to the fact that the molecules are adsorbed onto the surface at a parallel configuration, leading to a very small molecular dipole moment normal to the surface. The contribution of the surface geometry relaxation, $\Delta V_{geo.rel.}$, is also found to be small, at ≈0.08 eV and –0.06 eV for the stoichiometric and under-stoichiometric surfaces, respectively. Thus, the large work-function change (–1.22 eV and –1.11 eV) for both interfaces is found to be associated with the contribution of the interface dipole $\Delta V_{int.dip.}$, which is induced by a significant charge transfer from the CBP monolayer to the surface slab. This is confirmed by calculating the charge-density difference $\Delta\rho(y)$ averaged within the surface plane (*ac*-plane, as shown in Figure 3, with y representing the coordinates along the *b*-axis) between the interface system $\rho_{MoOx/CBP}(y)$ and each isolated component, $\rho_{MoOx}(y)$ and $\rho_{CBP}(y)$, and evaluating the induced potential energy change by solving the Poisson equation:

$$\frac{d^2V(y)}{dy^2} = -\frac{1}{\varepsilon_0}\Delta\rho(y) \quad (1)$$

where $V(y)$ is the electrostatic potential energy and ε_0 the vacuum permittivity. The amount of charge transfer $\Delta Q(y)$ is estimated by integrating the charge-density difference $\Delta\rho(y)$ along the y-direction and partitioning it between the surface slab and the CBP monolayer. Although a number of different partitioning schemes are available,[30] here, we chose to equally divide the empty space between the top oxygen layer of MoO_3 or MoO_x and the bottom carbon atoms of the CBP molecules.

Figure 11 displays the calculated results for both the MoO_3/CBP and MoO_x/CBP interfaces. In both cases, an increase in electron density, that is, a positive $\Delta\rho$, is observed near the top oxygen layer of the MoO_3 or MoO_x slab while a decrease, that is, a negative $\Delta\rho$, is obtained near the location of the CBP molecules; this points to an electron transfer from the CBP molecules to the MoO_3 and MoO_x slab. This is further confirmed by the integration of the charge-density difference, ΔQ, leading to an estimated electron transfer of ≈0.39 electrons per molecule for the MoO_3/CBP interface and 0.28 electrons per molecule for the MoO_x/CBP interface. Interestingly, the amount of electron transfer at the MoO_x/CBP interface is about 0.1 electrons lower than at the MoO_3/CBP interface; this can be attributed to the electron-donor nature of the oxygen vacancy on the MoO_x surface, which partially counteracts the electron transfer from the CBP molecules to the surface.

The contribution of the interface dipole ($\Delta V_{int.dip.}$) to the total work-function change for the two interfaces is given in the bottom panel of Figure 11a,b. In line with the extents of charge transfer, the contribution of $\Delta V_{int.dip.}$ at the MoO_3/CBP interface is –1.31 eV, about 0.3 eV larger, in absolute value, than the $\Delta V_{int.dip.}$ for the MoO_x/CBP interface, –1.00 eV. The summations of the three components (ΔV_{mol}, $\Delta V_{geo.rel.}$, and $\Delta V_{int.dip.}$) are –1.22 and –1.06 eV for the MoO_3/CBP and MoO_x/CBP interfaces, respectively, in excellent agreement with the DFT-calculated work-function changes for both interfaces (–1.22 and –1.11 eV, respectively). This further confirms the reliability of the DFT-derived work-function change and the decomposition mechanism developed in our earlier work.

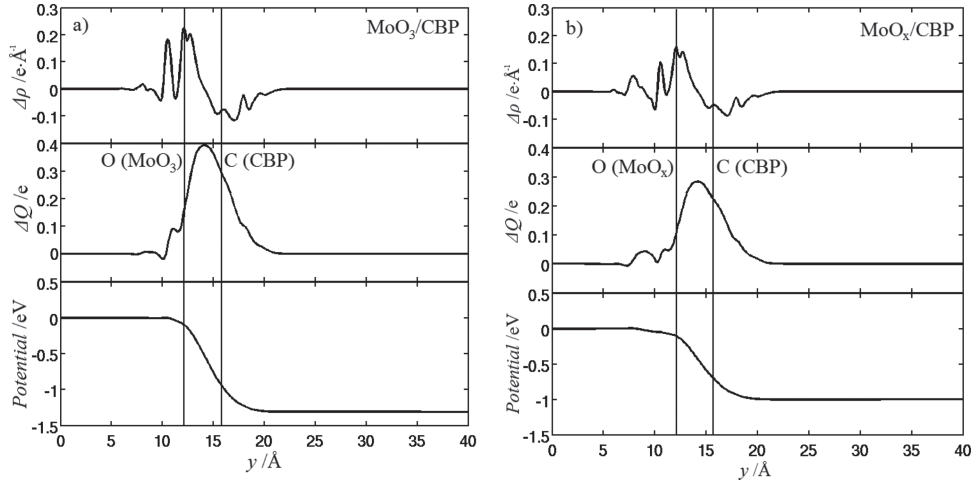

Figure 11. Charge-density difference, charge transfer, and contribution of the interface dipole for a) the MoO_3/CBP and b) MoO_x/CBP interfaces. The two vertical lines in both (a) and (b) indicate, respectively, the location of the highest oxygen in the MoO_3, MoO_x slab and the lowest carbon in the CBP molecular layer.

4. Conclusions

In this work, we have conducted a joint theoretical and experimental investigation of the interfacial electronic properties of the stoichiometric and under-stoichiometric MoO_3 surface with an organic adsorbate, namely CBP. We have considered different types of oxygen vacancies at the MoO_x ($x = 2.94$) surface, which are found to correspond to electron donor states located right below the CB edge or almost at mid-gap. The theoretical calculations point to an enhancement of the gap states after adsorption of CBP and show that part of the effect originates from states belonging to the organic adsorbate. The broad gap states observed experimentally for both bare and CBP-adsorbed MoO_x surfaces are thus attributed to: a) different types of oxygen vacancies in the metal-oxide, and b) molecular states contributed by the organic adsorbate.

The HOMO of CBP is found to almost align with the E_F, leading to a nearly zero barrier for electron collection and hole injection for both MoO_3 and MoO_x surfaces. Due to this favorable energy level alignment related to effective charge injection at the very interface, we indicate that, regardless of the existence of gap states below the CB edge, molybdenum trioxide can be a suitable candidate to realize efficient hole-injection and hole-collection in metal-oxide/organic interfaces.

Supporting Information

Supporting Information is available from the Wiley Online Library or from the author.

Acknowledgements

This work was supported as part of the Center for Interface Science: Solar Electric Materials (CISSEM), an Energy Frontier Research Center funded by the U.S. Department of Energy, Office of Science, Basic Energy Sciences, under Award Number DE-SC0001084. The computations reported here were performed mainly at Georgia Tech's "Center for Computational Molecular Science and Technology", funded through an NSF CRIF award (Grant No. CHE-0946869) and by the Georgia Institute of Technology.

Received: April 30, 2013
Published online: July 2, 2013

[1] a) S. Tokito, K. Noda, Y. Taga, *J. Phys. D: Appl. Phys.* **1996**, *29*, 2750; b) G. L. Frey, K. J. Reynolds, J. A. Barker, N. C. Greenham, R. H. Friend, *Appl. Phys.* **2002**, *92*, 7556; c) C. W. Chu, C. W. Chen, S. H. Li, E. H. E. Wu, Y. Yang, *Appl. Phys. Lett.* **2005**, *86*, 253503; d) J. Meyer, S. Hamwi, T. Bulow, H. H. Johannes, T. Riedl, W. Kowalsky, *Appl. Phys. Lett.* **2007**, *91*, 113506; e) L. M. Chen, Z. R. Hong, G. Li, Y. Yang, *Adv. Mater.* **2009**, *21*, 1434.
[2] M. Kröger, S. Hamwi, J. Meyer, T. Riedl, W. Kowalsky, A. Kahn, *Org. Electron.* **2009**, *10*, 932.
[3] J. Subbiah, G. Sarasqueta, F. So, H. J. Ding, I. Irfan, Y. L. Gao, D. Y. Kim *Appl. Phys. Lett.* **2009**, *95*, 093304.
[4] M. Kröger, S. Hamwi, J. Meyer, T. Riedl, W. Kowalsky, A. Kahn, *Appl. Phys. Lett.* **2009**, *95*, 123301.
[5] J. Meyer, S. Hamwi, M. Kröger, W. Kowalsky, T. Riedl, A. Kahn, *Adv. Mater.* **2012**, *24*, 5408.
[6] M. Vasilopoulou, L. C. Palilis, D. G. Georgiadou, S. Kennou, I. Kostis, D. Davazoglou, P. Argitis, *Appl. Phys. Lett.* **2012**, *100*, 013311.
[7] J. Hwang, A. Wan, A. Kahn, *Mater. Sci. Eng., R* **2009**, *64*, 1.
[8] a) G. Kresse, J. Furthmüller, *Phys. Rev. B* **1996**, *54*, 11169; b) G. Kresse, J. Furthmüller, *Comput. Mater. Sci.* **1996**, *6*, 15.
[9] J. P. Perdew, K. Burke, M. Ernzerhof, *Phys. Rev. Lett.* **1997**, *78*, 1396.
[10] a) P. E. Blöchl, *Phys. Rev. B* **1994**, *50*, 17953; b) G. Kresse, D. Joubert, *Phys. Rev. B* **1999**, *59*, 1758.
[11] L. Kihlborg, *Z. Kristallogr.* **1964**, *21*, 443.
[12] X. Yin, H. Han, A. Miyamoto, *J. Mol. Model.* **2001**, *7*, 207.
[13] F. Cora, A. Patel, N. M. Harrison, C. Roetti, R. A. C. Catlow, *J. Mater. Chem.* **1997**, *7*, 959.
[14] R. Coquet, D. J. Willock, *Phys. Chem. Chem. Phys.* **2005**, *7*, 3819.

[15] a) M. Chen, U. V. Waghmare, C. M. Friend, E. Kaxiras, *J. Chem. Phys.* **1998**, *109*, 6854; b) R. Tokarz-Sobieraj, K. Hermann, M. Witko, A. Blume, G. Mestl, R. Schlögl, Surf. Sci. 2001, 489, 107.
[16] D. O. Scanlon, G. W. Watson, D. J. Payne, G. R. Atkinson, R. G. Egdell, D. S. L. Law, *J. Phys. Chem. C* **2010**, *114*, 4636.
[17] K. Momma, F. Izumi, *J. Appl. Crystallogr.* **2011**, *44*, 1272.
[18] K. Kanai, K. Koizumi, S. Ouchi, Y. Tsukamoto, K. Sakanoue, Y. Ouchi, K. Seki, *Org. Electron.* **2010**, *11*, 188.
[19] M. T. Greiner, L. Chai, M. G. Helander, W.-M. Tang, Z.-H. Lu, *Adv. Funct. Mater.* **2012**, *22*, 4557.
[20] S. R. Hammond, J. Meyer, N. E. Widjonarko, P. F. Ndione, A. K. Sigdel, A. Garcia, A. Miedaner, M. T. Lloyd, A. Kahn, D. S. Ginley, J. J. Berry, D. C. Olson, *J. Mater. Chem.* **2012**, *22*, 3249.
[21] J. Meyer, A. Shu, M. Kröger, A. Kahn, *Appl. Phys. Lett.* **2010**, *96*, 133308.
[22] I. Irfan, H. J. Ding, Y. L. Gao, C. Small, D. Y. Kim, J. Subbiah, F. So, *Appl. Phys. Lett.* **2010**, *96*, 243307.
[23] a) C. Girotto, E. Voroshazi, D. Cheyns, P. Heremans, B. P. Rand, *ACS Appl. Mater. Interfaces* **2011**, *3*, 3244; b) K. Zilberberg, H. Gharbi, A. Behrendt, S. Trost, T. Riedl, *ACS Appl. Mater. Interfaces* **2012**, *4*, 1164.
[24] a) J. Meyer, R. Khalandovsky, P. Görrn, A. Kahn, *Adv. Mater.* **2011**, *23*, 70; b) I. Irfan, A. J. Turinske, Z. Bao, Y. Gao, *Appl. Phys. Lett.* **2012**, *101*, 093305.
[25] S. W. Cho, L. F. J. Piper, A. DeMasi, A. R. H. Preston, K. E. Smith, K. V. Chauhan, R. A. Hatton, T. S. Jones, *J. Phys. Chem. C* **2010**, *114*, 18252.
[26] P. B. Paramonov, S. A. Paniagua, P. J. Hotchkiss, S. C. Jones, N. R. Armstrong, S. R. Marder, J.-L. Brédas, *Chem. Mater.* **2008**, *20*, 5131.
[27] P. J. Hotchkiss, H. Li, P. B. Paramonov, S. A. Paniagua, S. C. Jones, N. R. Armstrong, J.-L. Brédas, S. R. Marder, *Adv. Mater.* **2009**, *21*, 4496.
[28] I. Hancox, P. Sullivan, K. V. Chauhan, N. Beaumont, L. A. Rochford, R. A. Hatton, T. S. Jones, *Org. Electron.* **2010**, *11*, 2019.
[29] a) G. Heimel, L. Romaner, J.-L. Brédas, E. Zojer, *Surf. Sci.* **2006**, *600*, 4548; b) G. Heimel, L. Romaner, J.-L. Brédas, E. Zojer, *Phys. Rev. Lett.* **2006**, *96*, 196806; c) G. Heimel, L. Romaner, E. Zojer, J.-L. Brédas, *Nano Lett.* **2007**, *7*, 932; d) G. Heimel, L. Romaner, E. Zojer, J.-L. Brédas, *Acc. Chem. Res.* **2008**, *41*, 721; e) H. Li, P. Paramonov, J.-L. Brédas, *J. Mater. Chem.* **2010**, *20*, 2630; f) H. Li, P. Winget, J.-L. Brédas, *Adv. Mater.* **2012**, *24*, 687; g) C. Wood, H. Li, P. Winget, J.-L. Brédas, *J. Phys. Chem. C* **2012**, *116*, 19125.
[30] R. F. W. Bader, *Acc. Chem. Res.* **1985**, *18*, 9.